Research Article

Huseyin Ozan Tekin*, Ghada ALMisned*, Yasser Saad Rammah, Gulfem Susoy, Fatema T. Ali, Duygu Sen Baykal, Hesham M. H. Zakaly#, Shams A. M. Issa, Antoaneta Ene*

Mechanical properties, elastic moduli, transmission factors, and gamma-ray-shielding performances of Bi_2O_3–P_2O_5–B_2O_3–V_2O_5 quaternary glass system

https://doi.org/10.1515/chem-2022-0145
received February 2, 2022; accepted March 8, 2022

Abstract: Mechanical properties, elastic moduli, transmission factors (TFs), and gamma-ray shielding performance of quaternary glass systems with chemical composition $(0.25–x)Bi_2O_3–xB_2O_3–0.75(50\%P_2O_5–50\%V_2O_5)$, where x = 0.05 (S1), 0.10 (S2), 0.15 (S3), and 0.20 (S4) mol%, were comprehensively studied. The MCNPX code, Phy-X/PSD software, and the Makishima–Mackenzie model were utilized to achieve the mentioned purposes. The values of the packing density (V_t) decreased from 0.634432 to 0.600611, while those of the dissociation energy (G_t) increased from 51.6125 kJ/cm^3 for the S1 glass sample (with Bi_2O_3 = 5 mol%) to 56.7525 kJ/cm^3 for the S4 glass sample (with Bi_2O_3 = 20 mol%). This means that the mechanical properties were enhanced by increasing the Bi_2O_3 content in glasses. Linear (μ) and mass attenuation (μ_m) coefficients for the S4 glass sample were the greatest compared to those for glass materials investigated, i.e., $(\mu, \mu_m)_{S1} < (\mu, \mu_m)_{S2} < (\mu, \mu_m)_{S3} < (\mu, \mu_m)_{S4}$. Half- and tenth-value layers (HVL and TVL, respectively) follow the trend: $(HVL, TVL)_{S1} > (HVL, TVL)_{S2} > (HVL, TVL)_{S3} > (HVL, TVL)_{S4}$. The effective atomic number (Z_{eff}) of investigated glasses has the same trend as of linear and mass attenuation coefficients. Our findings indicate that increasing the amount of Bi_2O_3 reinforcement decreased the exposure buildup factor and energy absorption buildup factor values for all mean free path values (0.5–40 mfp). All glasses recorded the minimum TF values at a thickness of 3 cm. The findings would benefit the scientific community in determining the most appropriate additive bismuth(III) oxide/diboron trioxide type and related glass composition to provide the shielding properties previously mentioned in terms of needs and utilization requirements, as well as the most suitable glass composition.

Keywords: quaternary glasses, transmission factors, MCNPX, Makishima–Mackenzie model

The researcher (Hesham M.H. Zakaly) is funded by a scholarship under the Joint Executive Program between Egypt and Russia.

*** Corresponding author: Huseyin Ozan Tekin,** Department of Medical Diagnostic Imaging, College of Health Sciences, University of Sharjah, 27272, Sharjah, United Arab Emirates; Istinye University, Faculty of Engineering and Natural Sciences, Computer Engineering Department, Istanbul 34396, Turkey, e-mail: tekin765@gmail.com
*** Corresponding author: Ghada ALMisned,** Department of Physics, College of Science, Princess Nourah Bint Abdulrahman University, P.O. Box 84428, Riyadh 11671, Saudi Arabia, e-mail: gaalmisned@pnu.edu.sa
*** Corresponding author: Antoaneta Ene,** Department of Chemistry, Physics and Environment, INPOLDE Research Center, Faculty of Sciences and Environment, Dunarea de Jos University of Galati, 47 Domneasca Street, 800008 Galati, Romania, e-mail: antoaneta.ene@ugal.ro
Yasser Saad Rammah: Department of Physics, Faculty of Science, Menoufia University, Shebin El-Koom 32511, Menoufia, Egypt
Gulfem Susoy: Department of Physics, Faculty of Science, Istanbul University, Istanbul 34134, Turkey
Fatema T. Ali: Center for Advanced Materials Research, Research Institute of Sciences and Engineering, University of Sharjah, Sharjah 27272, United Arab Emirates
Duygu Sen Baykal: Istanbul Kent University, Vocational School of Health Sciences, Medical Imaging Techniques, Istanbul, 34433, Turkey
Hesham M. H. Zakaly: Institute of Physics and Technology, Ural Federal University, 620002 Ekaterinburg, Russia; Physics Department, Faculty of Science, Al-Azhar University, Assiut 71524, Egypt
Shams A. M. Issa: Physics Department, Faculty of Science, University of Tabuk, Tabuk 47512, Saudi Arabia; Physics Department, Faculty of Science, Al-Azhar University, Assiut 71524, Egypt

1 Introduction

Ionizing radiations (particle and electromagnetic) are increasingly used in medical and industrial applications for various purposes. The advantages of these radiations

are increasingly being used in electric power generation, radiotherapy, medical diagnosis, nuclear power, and many industrial operations. Several organizations and institutes have developed guidelines for safely using and dealing with this type of radiation. Time, distance, and shielding are the three basic concepts of radiation protection [1–5]. The efficiency of shielding materials can be improved by increasing absorption of these materials to different types of ionizing radiations. For many years, lead (Pb) and concrete have been considered ideal shielding materials. Toxic properties, opacity, installation difficulties, and space consumption are only the few disadvantages and concerns of these two materials. Glass shielding is logical when clear protection against ionizing radiations is required [6–8]. Borate-based glasses are fascinating optical materials because of their exceptional and unique properties, including high transparency, high thermal stability, low cost, and low melting temperature points [9,10]. Many applications of oxide-based glasses in various science disciplines have sparked research interest on these materials. The study of vitrified materials is now considered a subset of the larger area of materials science. The use of alkaline oxides to modify borate glasses is particularly intriguing. Heavy elements and oxides are added to the borate-glass network as modifiers to improve the radiation absorption performance of the material. Among the several types of oxides, bismuth oxide (Bi_2O_3) has excellent compatibility with borate glasses. Bi_2O_3 is the utmost substitute for toxic lead oxide because it forms glasses easily [11]. Lakshminarayana et al. [12] have investigated the effect of Bi_2O_3 in compositions B_2O_3–Bi_2O_3–CaO and B_2O3–Bi_2O_3–SrO on radiation shielding properties using MCNPX, Geant4, and Penelope codes. They concluded that increasing the amount of Bi_2O_3 resulted in an improvement in shielding properties. The results obtained by Alsaif et al. [13] further indicate that glass (compositionally graded Pb-free lithium borate glass) has demonstrated its support of a superior-ray shielding effectiveness compared to the other types of glasses tested [14]. The physical and optical properties of glass systems are improved by combining other glass formers such as SiO_2, B_2O_3, P_2O_5, and GeO_2 [15–17]. Phosphate (P_2O_5)-based glasses, on the other hand, are attractive materials for opto-electronic and electronic equipment due to their environmental friendliness, low melting temperatures, good UV-transmittance qualities, and high thermal expansion [18]. In a similar way, combining phosphate glasses with boron oxide improves durability. Both phosphate and borate glasses have poor chemical resistance, which is critical for their practical applications [19,20]. Simultaneously, it was discovered that adding B_2O_3 to phosphate glasses or P_2O_5 to borate glasses improves chemical stability by forming P–O–B bonds in the glass network [21–23]. The addition of B_2O_3 to phosphate glasses improves their mechanical [24] and optical [25] properties while also increasing their ionic conductivity [26].

Furthermore, while adding boron oxide to the phosphate network initially reduces the potential for crystallization, borophosphate glasses with a high B_2O_3 content have lower thermal stability [27]. The development of new glasses with unusual properties and unique applications, such as biological materials, sealing and packaging materials, solid electrolytes, and so on, demonstrates the progress in the study of borophosphate glasses [28–30]. Many researchers have recently thrown light on the importance of transition-metal oxides (TMO) as glass modifiers. Vanadium oxide (V_2O_5) is a smart TMO that may be used as a conditioned glass former and has excellent electrical and optical properties [31–33]. Because of their wider glass-forming region and potential technological uses, V_2O_5 glasses have been regarded as a new branch in semiconducting glasses [34,35]. Radiation shielding parameters may be calculated theoretically using Phy-X/PSD [36]. Several researchers previously evaluated the mass attenuation coefficient factor (μ/ρ), HVL, mean free path (mfp), effective atomic number (Z_{eff}), and other parameters to see whether borate glasses could be used as γ-radiation protective materials [37–39]. The various types of bismuth(III) oxide/diboron trioxide reinforcements used to optimize the glass's features were hypothesized to change the glass's fundamental nuclear radiation shielding, mechanical properties, elastic moduli, and transmission factor (TF) qualities. As a result, we wanted to see how bismuth(III) oxide/diboron trioxide additions affected these glasses' nuclear radiation shielding and mechanical properties. The goal of this research is to develop a new, highly efficient, and environmentally friendly shielding material that may be used in nuclear medicine units to replace lead or lead-based shielding materials. The efficiency and quality of each sample will be examined and debated as the additive concentration increases. The current study determined and detailed the shielding properties of gamma rays and neutron beams associated with the Bi_2O_3–P_2O_5–B_2O_3–V_2O_5 quaternary glass system, as well as several key physical and mechanical aspects. The findings of this inquiry could be used in future investigations or added to prior ones with the same goal.

2 Materials and methods

2.1 Studied glasses

In this article, four glass samples of bismo-vanadio-borophosphate with chemical composition $(0.25-x)Bi_2O_3–xB_2O_3–0.75(50\% P_2O_5–50\% V_2O_5)$, where x = 0.05, 0.10, 0.15, and 0.20, were selected from ref. [40]. The studied samples are coded as follows:

- **S1:** $0.05Bi_2O_3–0.20B_2O_3–0.75(50\% P_2O_5–50\% V_2O_5)$ with a density of 3.158 (g/cm^3) and a molar volume of 50.226 (cm^3/mol).
- **S2:** $0.10Bi_2O_3–0.15B_2O_3–0.75(50\% P_2O_5–50\% V_2O_5)$ with a density of3.501 (g/cm^3) and a molar volume of 50.973 (cm^3/mol).
- **S3:** $0.15Bi_2O_3–0.10B_2O_3–0.75(50\% P_2O_5–50\% V_2O_5)$ with a density of 3.690 (g/cm^3) and a molar volume of 53.724 (cm^3/mol).
- **S4:** $0.20Bi_2O_3–0.05B_2O_3–0.75(50\% P_2O_5–50\% V_2O_5)$ with a density of 4.010 (g/cm^3) and a molar volume of 54.378 (cm^3/mol).

Sample codes, elemental weight fractions, densities, and molar volumes of the investigated glasses are given in Table 1.

2.2 Elastic moduli and Poisson's ratio

Poisson's ratios (σ_{M-M}) and elastic moduli (shear [S_{M-M}], Young's moduli [E_{MM}], bulk moduli [K_{M-M}], and longitudinal moduli (L_{M-M})) of the studied (S1–S4) glasses were computed using the Makishima–Mackenzie (M–M) formulas [41–45]. The M–M principle mainly depends on the packing density factor (V_i) and the dissociation energy per unit volume (G_i) for the glass system oxides (here, Bi_2O_3, B_2O_3, P_2O_5, and V_2O_5). The G_i and V_i values of these oxides are tabulated in Table 2. The computed formulas of (σ_{M-M}), (S_{M-M}), (E_{M-M}), (K_{M-M}), and (L_{M-M}) are given in Table 3.

Table 2: Packing density factor (V_i) and dissociation/bond energy per unit volume (G_i) of the oxides Bi_2O_3, B_2O_3, P_2O_5, and V_2O_5

Oxide	V_i (cm^3/mol) [32,33]	G_i (kJ/cm^3) [32,33]
Bi_2O_3	26.1	31.6
B_2O_3	20.8	16.4
P_2O_5	34.8	62.8
V_2O_5	35.6	69.5

2.3 Monte Carlo simulation phase and studied gamma-ray-shielding properties

Including the fundamental gamma-ray-shielding capabilities, it is vital to assess the shielding materials' unique attenuation capacities when primary and secondary gamma rays are available. This technique could provide crucial data on the proportion of gamma rays transmitted through the attenuator medium. The term TF [46] is a critical metric that can assist in determining the aforementioned values in order to gain a better understanding of shielding materials' attenuation properties against ionizing gamma rays. The TF of the studied glasses was determined in this study using the Monte Carlo simulation algorithm MCNPX [47] (version 2.7.0). The ratio of the radiation flux (F) flowing through the material medium to the flux incident on the absorber's surface is the TF value attributed to a specific absorber. The mean gamma-ray flux in the F4 tally mesh is divided by the mean gamma-ray flux in the uniform detection field to get the TF of the analyzed glasses. Two detecting fields are positioned in front and behind the glass to convert this formulation to the MCNPX code. While the intensity of primary gamma rays was measured on the right front of the glass material, the intensity of

Table 1: Sample code, elemental weight fraction, density, and molar volume of $(0.25-x)Bi_2O_3–xB_2O_3–0.75(50\% P_2O_5–50\% V_2O_5)$, where x = 0.05, 0.10, 0.15, and 0.20 glasses

Sample code	Elemental weight fraction (wt%)					Density (g/cm^3) [31]	Molar volume (cm^3/mol) [31]
	B	O	P	V	Bi		
S1	0.027254	0.453788	0.146422	0.240816	0.13172	3.1589	50.2263
S2	0.018171	0.403401	0.130164	0.214076	0.234189	3.5016	50.9738
S3	0.010903	0.363085	0.117155	0.192681	0.316176	3.6909	53.7240
S4	0.004956	0.330095	0.10651	0.175174	0.383264	4.0108	54.3781

Table 3: Total ionic packing density (V_t), total dissociation energy (G_t), Young's modulus (E_{M-M}), bulk modulus (K_{M-M}), shear modulus (S_{M-M}), and Poisson's ratio (σ_{M-M}) based on the Makishima–Mackenzie model of the studied glasses.

Parameters and elastic moduli	S1	S2	S3	S4
$V_t = \left(\frac{1}{V_m}\right)\sum_i (V_i x_i)$	0.634432	0.630334	0.602989	0.600611
$G_t = \sum_i (G_i x_i)$ (kJ/cm^3)	51.6125	55.2325	55.9925	56.7525
$E_{M-M} = 2V_tG_t$ (GPa)	65.48928	69.62981	67.52576	68.1723
$K_{M-M} = 1.2\ V_tE_{M-M}$ (GPa)	49.85822	52.66802	48.86078	49.134
$S_{M-M} = (3E_{M-M}K_{M-M})/(9K_{M-M} - E_{M-M})$ (gPa)	25.56015	27.20641	26.59194	26.86585
$L_{M-M} = K_{M-M} + \frac{4}{3}S_{M-M}$ (GPa)	83.85322	88.85255	84.22806	84.86558
$\sigma_{M-M} = \left(\frac{E_{M-M}}{2G_{M-M}}\right) - 1$ (GPa)	0.281082	0.279658	0.269666	0.268754

The x_i is mole fraction of the component i of an oxide glass and V_m is the molar volume of the glass samples.

attenuated gamma rays flowing through the glass was measured immediately behind the glass. The MCNPX simulation setup for the gamma-ray TF is shown in Figure 1. As the first stage in the simulation approach, the geometry of the TF measurement was generated using the code's INPUT file. MCNPX's INPUT file is divided into three primary sections: a CELL card, a SURFACE card, and a DATA card. For example, we assessed the equipment's CELL structures by determining their covering surfaces and densities. Additionally, the CELL card component provides material identification numbers (Mn). After that, the geometrical orientations of the TF configuration's surfaces were used as input, as well as their geometrical structures, which may be planar, spherical, or cone. The DATA card section also incorporates radioisotope energies and the source geometry as a point isotropic source. All simulations were run using a Lenovo ThinkStation-P620/30E0008QUS Workstation-1x AMD-Ryzen, Threadripper PRO Hexadeca-core (16 Core) 3955WX 3.90 GHz–32 GB DDR4 SDRAM RAM.

3 Results and discussion

3.1 Mechanical characteristics

In order to evaluate Poisson's ratios and the elastic moduli of the investigated (S1–S4) glasses, first, the total ionic packing density (V_t) and total dissociation energy (G_t) of the contribution glass system oxides are computed and tabulated in Table 3. The values of V_t and G_t for S1–S4 glasses revealed that there is a slight decrease in V_t from 0.634432 for the S1 glass sample to 0.600611 for the S4 glass sample, as shown in Figure 2. The noted decrease may be attributed to the higher value of the ionic radius of Bi_2O_3 than that of B_2O_3. Therefore, increasing Bi_2O_3 in the S1–S4 glasses increases G_t of the system from 51.6125 kJ/cm^3 for the S1 glass sample (with Bi_2O_3 = 5 mol%) to 56.7525 kJ/cm^3 for the S4 glass sample (with Bi_2O_3 = 20 mol%), as shown in Figure 2. This is due to the substitution of B_2O_3, which has a dissociation energy of 16.4 kJ/cm^3, with Bi_2O_3, which has a dissociation energy of 31.6 kJ/cm^3. Second, Poisson's ratio (σ_{M-M}) and elastic moduli ([S_{M-M}], [E_{MM}], [K_{M-M}], and [L_{M-M}]) are computed for the studied glasses (S1–S4) and tabulated in Table 3. A slight variation in E_{M-M} from 65.48928 GPa for the S1 glass sample to 68.1723 GPa for the S4 glass sample, K_{M-M} from 48.86078 GPa for the S3 glass sample to 52.66802 GPa for the S2 glass sample, S_{M-M} from 25.56015 GPa for the S1 glass sample to 27.20641 GPa for the S2 glass sample, and L_{M-M} from 83.85322 GPa for the S1 glass sample to 88.85255 GPa for the S2 glass sample, respectively, is observed, as illustrated in Figure 3. Poisson's ratio decreases from 0.281082 (S1 glass sample) to 0.268754 (S4 glass sample) (Figure 4). The noted variation in the studied mechanical properties was attributed mainly to the increase in defects and vacancies and the formation of a large number of non-bridging oxygen with increasing Bi_2O_3 and decreasing B_2O_3 ratios in S1—S4 glasses [41–45].

3.2 Gamma-ray-shielding properties

Another phase of the characterization processes of the studied glass group was the multiple examinations of the shielding properties of four different glass samples with different parameters against ionizing gamma rays. The variation in the material densities of the studied glass group is shown in Figure 5. The figure shows a linear

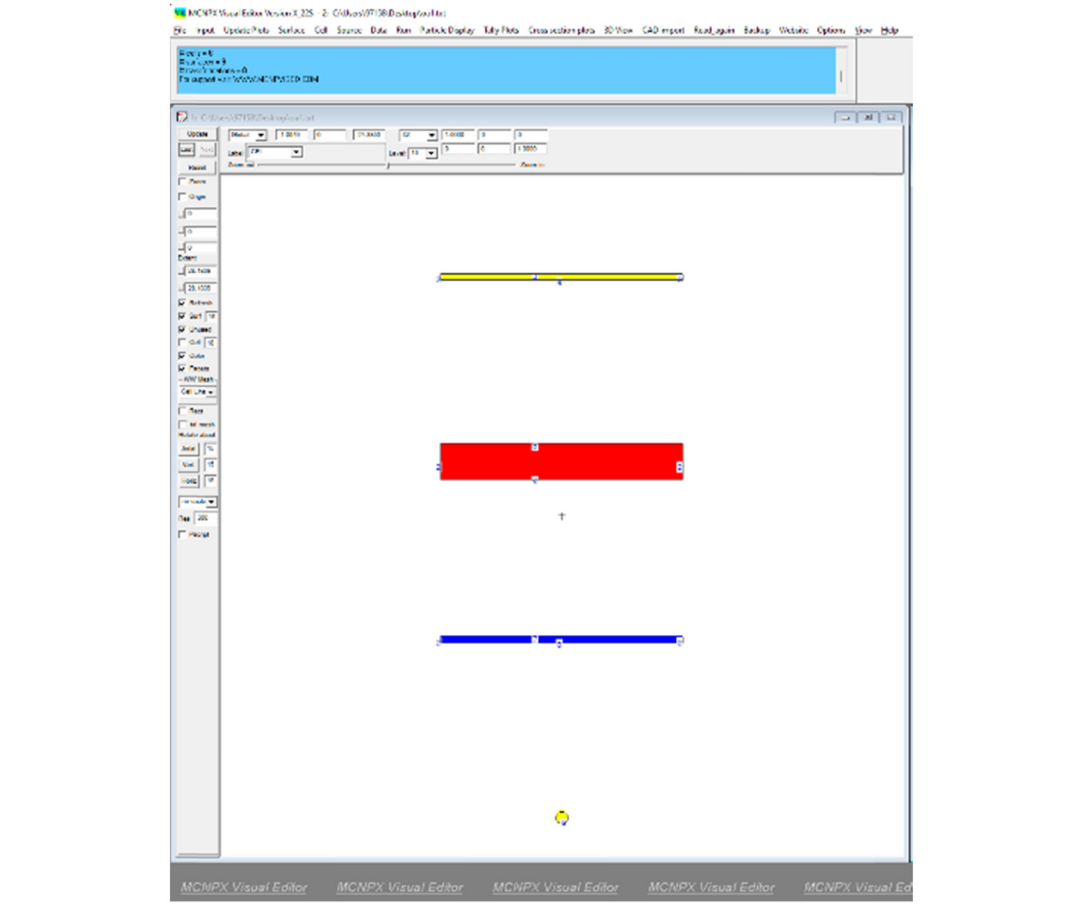

(a)

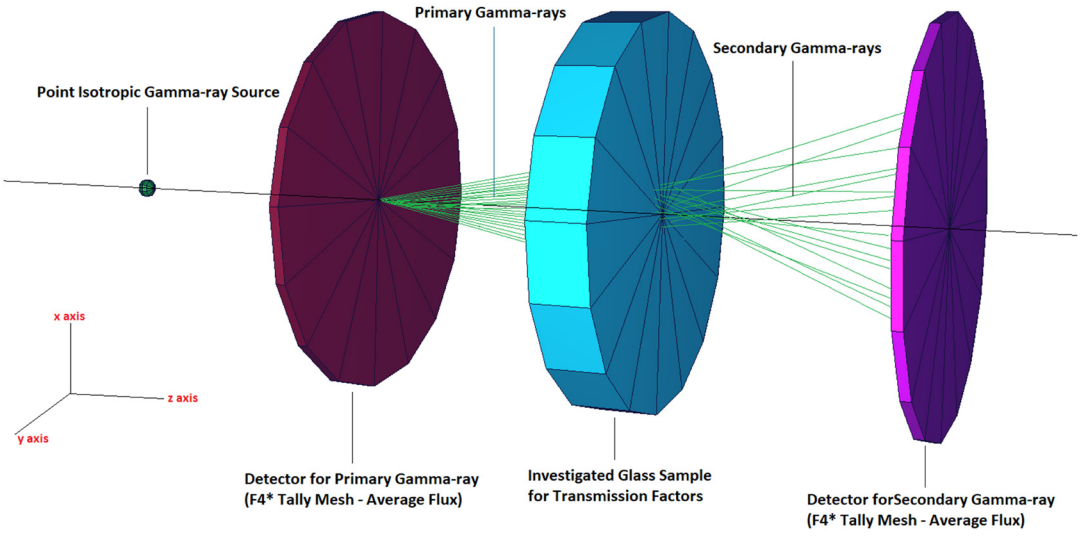

(b)

Figure 1: (a) 2-D view of the designed MCNPX simulation setup and (b) 3-D illustration of designed MCNPX setup (2-D and 3-D views are obtained from MCNPX Visual Editor VisedX22S).

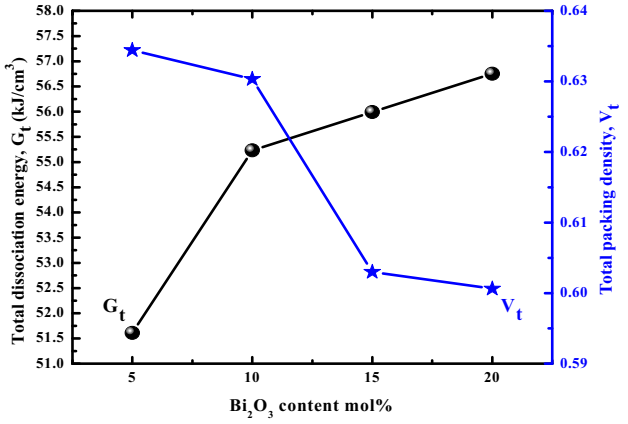

Figure 2: Variation of packing density and dissociation energy as a function of Bi_2O_3 content mol% for all S1–S4 glasses.

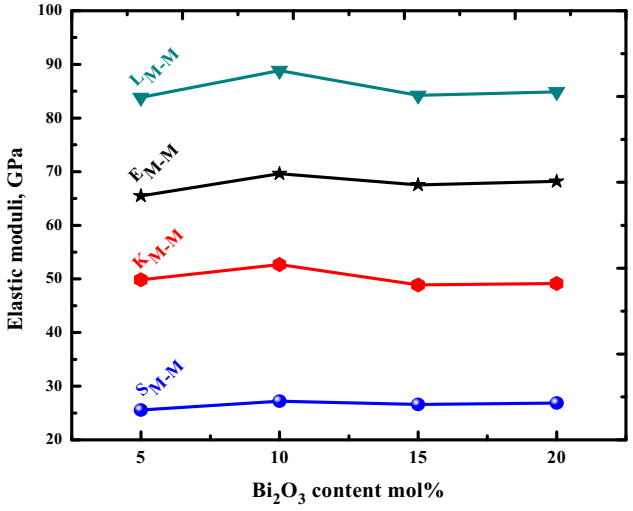

Figure 3: Variation of elastic moduli as a function of Bi_2O_3 content mol% for all S1–S4 glasses.

density increasing trend from sample S1 to sample S4. The primary reason for this rise is because the Bi additive rate in the S1 sample has been increasing consistently for each sample, resulting in the S4 sample having the highest Bi additive rate (0.383264 wt%). As a consequence of the influence of the highest Bi additive rate, the maximum glass density for the S4 sample was 4.0108 g/cm^3. Meanwhile, the term linear attenuation coefficient (μ) may be used to describe a significant parameter dependence on the material density and can be investigated for each energy value. Figure 6 illustrates the linear attenuation coefficient's fluctuation concerning various energy values and its representation as a function of increasing energy values. When an energetic photon interacts with matter, various types of interactions might dominate the process depending on the photon's energy. For instance, the

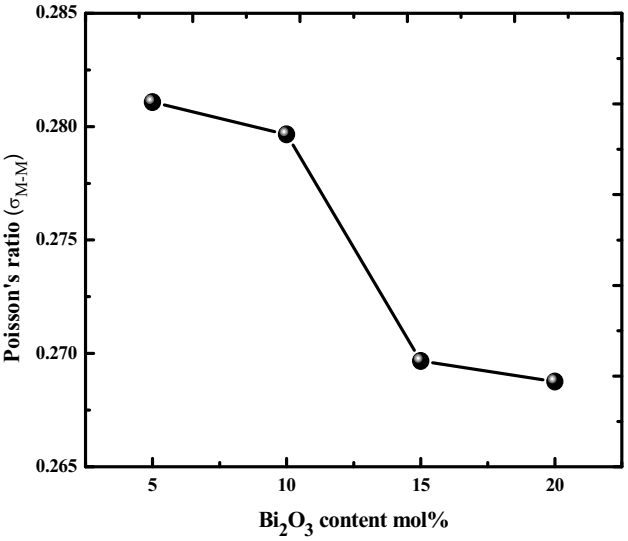

Figure 4: Variation of Poisson's ratios as a function of Bi_2O_3 content mol% for all S1–S4 glasses.

photoelectric effect is the most prevalent interaction in the low-energy area. As seen in Figure 6, the linear attenuation coefficients in the low-energy area have shown a strong downward trend, with some reports indicating a dramatic decrease. Following this decline, a peak in the value of the Bi k-absorption edge was found, and the linear attenuation coefficient values resumed their steady decline. We reported the highest linear attenuation coefficients for the S4 sample among the glass materials investigated. The primary reason for this situation is the maximum Bi contribution described above, as well as the indirect effect of the additive on

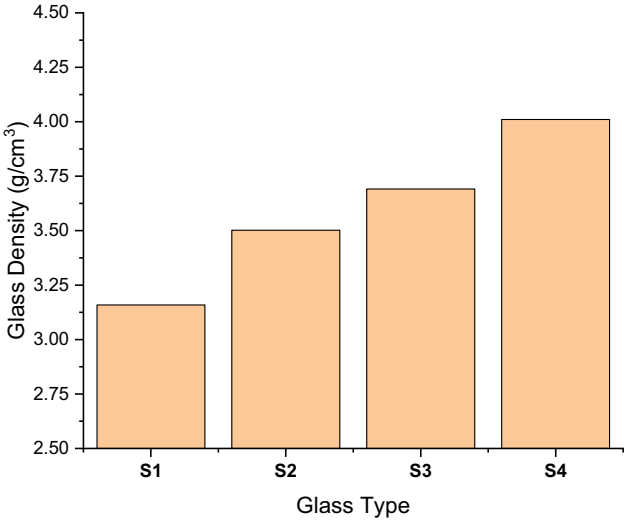

Figure 5: Variation of investigated glass densities.

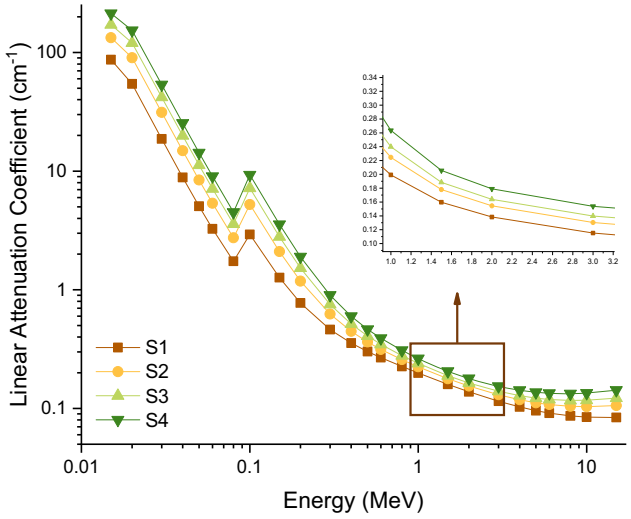

Figure 6: Variation of linear attenuation coefficient (cm^{-1}) with photon energy (MeV) for all S1–S4 glasses.

glass density. Next, we calculated another essential gamma-ray-shielding parameter, a density-independent parameter, namely, mass attenuation coefficient (μ_m). Figure 7 shows the variation in mass attenuation coefficients (cm^2/g) with photon energy (MeV) for all S1–S4 glasses. In general, we observed comparable behaviors, such as linear attenuation coefficients, over a range of gamma-ray energy areas, including low, mid, and high. On the other hand, the S4 sample showed the highest mass attenuation coefficient values among the investigated glasses. This may be explained by the fact that the highest proportion of Bi in the structure of S4 has influenced the attitude of mass attenuation coefficients due to its higher atomic number. The HVL is one of the practical definitions that include the attenuation that occurs as a consequence of shielding materials interacting with gamma rays at the atomic level. In principle, the HVL result represents the material thickness at which the intensity of the gamma ray affecting the shielding material is reduced to half [48,49]. Therefore, materials that halve the same gamma-ray intensity at lower thicknesses can be considered superior in terms of shielding properties [50–57]. The HVL values of the glass samples studied in this research were determined to be in the energy range of 0.015–15 MeV. The HVL values of samples S1, S2, S3, and S4 are shown in Figure 8 as a function of the incoming gamma-ray energy values. As can be seen, the examined glass samples showed notable variations in behavior as the photon energy increased the thickness of the HVL. For example, although the half-value thicknesses are minimal in the low-energy zone, they increase proportionately as the energy increases. The fundamental reason seems to be that the intensity of low-energy photons may be reduced by a factor of two at very thin layers due to their poor penetrating abilities. Due to the glass's density and weight, the required half-value thickness for the low-energy region is very minimal for all the glass samples investigated. However, as seen in the graph, these thickness values increase up to the range of 3–4 cm in the high-energy zone. As seen in Figure 8, the S4 sample has the lowest HVL values at all energy values. As a result of the S4 sample's attenuation coefficients, it is understood that it performs the halving process at the smallest thickness possible among all the glass samples examined for given radiation

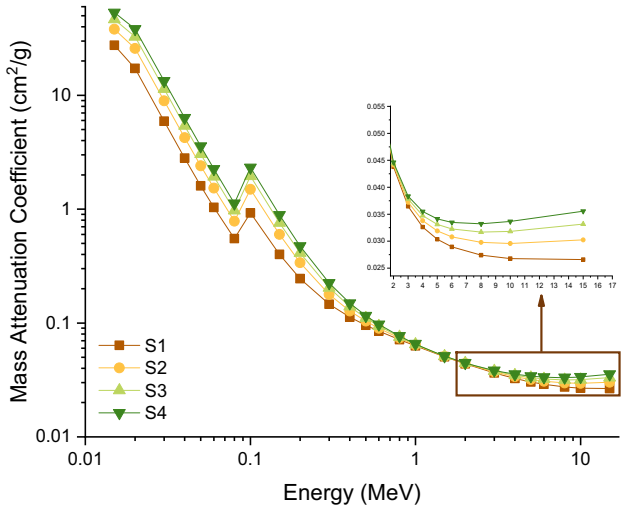

Figure 7: Variation of mass attenuation coefficients (cm^2/g) with photon energy (MeV) for all S1–S4 glasses.

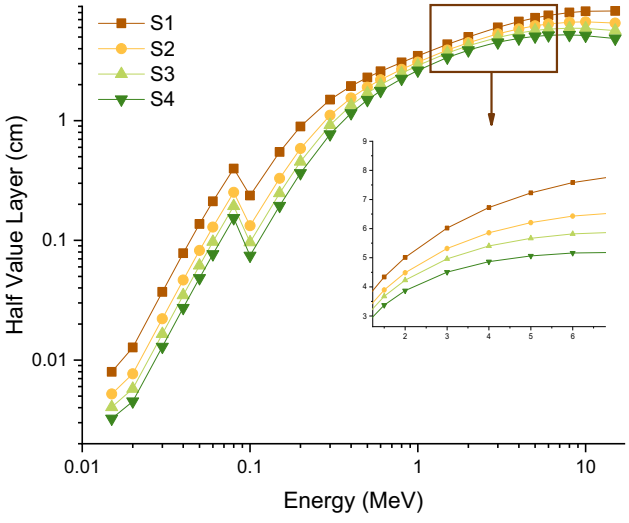

Figure 8: Variation of HCL (cm) with photon energy (MeV) for all S1–S4 glasses.

energy by taking the lowest values in the half-value thickness values directly related to these coefficients. On the other hand, a TVL may be used to create another component that is identical to the HVL and gives comparable functioning information. As HVL, this parameter defines the thickness of material required to lower the radiation intensity on the material by one-tenth [38,39]. Figure 9 illustrates the energy-dependent fluctuation in the one-tenth thickness of the examined heavy metal oxide glasses. As can be observed, TVL values have larger quantitative values compared to HVL values for identical energy values. This is a normal occurrence, and there is a requirement for greater shielding material to limit the radiation intensity with a particular energy value to one-tenth. Although these two characteristics have quantitative values that vary for the same energy values, the study's findings indicate that the S4 sample also has the lowest one-tenth value thickness values. Including these two critical properties, the S4 sample will provide minimal HVL and TVL thicknesses in any process operating between 0.015 and 15 MeV photon energy. This reveals that among the glass samples studied, employing the S4 sample is the most beneficial at the lowest cost and with the least physical space occupied by the glass shielding sample. Individual interactions between the photon and the material atoms begin inside the material after the first contact of the radiation with the shielding material and its penetration into the interior regions. As a consequence of these interactions, the incoming radiation loses energy, and total absorption occurs when the energy is reduced to zero. The mfp parameter determines the required space between two successive photon interactions in a material [25–29]. The mfp can be computed for a given energy value, and it offers crucial information about how doping and chemical composition changes impact the following interaction distance, which is especially valuable in comparison-based research. The change in the mfp (cm) as a function of photon energy (MeV) is shown in Figure 10 for all S1–S5 glasses. As seen in Figure 10, the mfp values of the examined glass samples vary according to the incoming photon energy (MeV). This offers compelling evidence for a relationship between the penetrating properties of gamma rays and mean distance traveled by gamma rays. Even though the mfp value increases with gamma-ray energy, the S4 sample exhibited

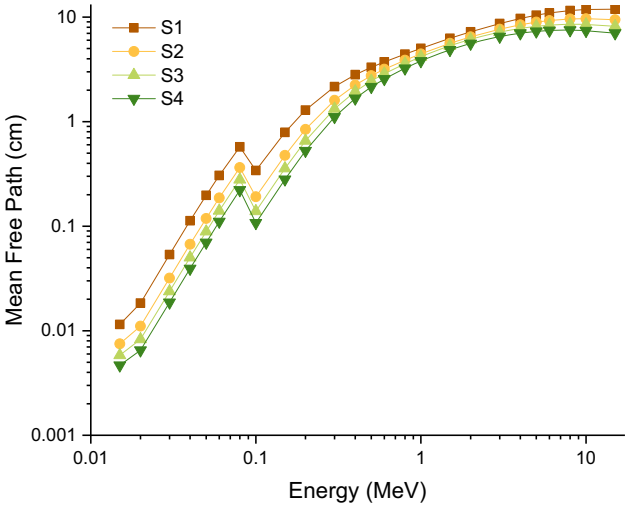

Figure 10: Variation of mfp (cm) with photon energy (MeV) for all S1–S4 glasses.

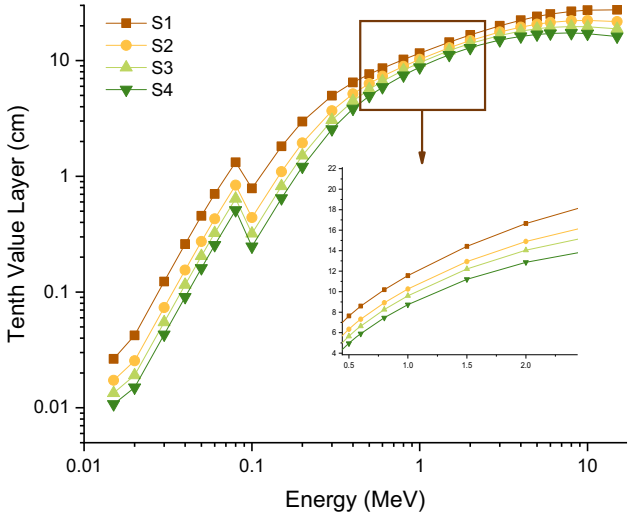

Figure 9: Variation of TVL (cm) with photon energy (MeV) for all S1–S4 glasses.

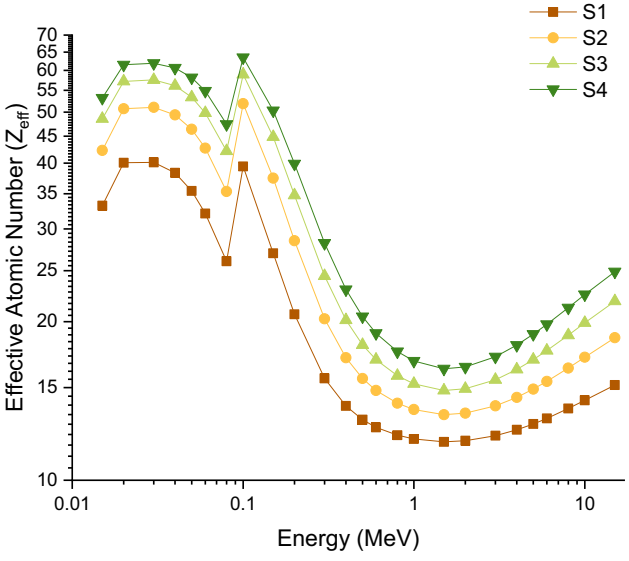

Figure 11: Variation of effective atomic number (Z_{eff}) with photon energy (MeV) for all S1–S4 glasses.

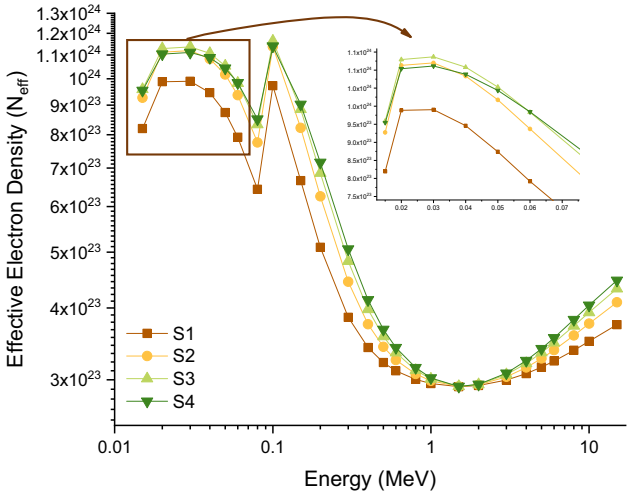

Figure 12: Variation of effective electron density (electrons/g) with photon energy (MeV) for all S1–S4 glasses.

the lowest mfp values for a given gamma-ray energy. In other words, gamma rays of certain energy may interact in close proximity inside the S4 sample and are therefore more effectively absorbed by the material. The fluctuation of the effective atomic number (Z_{eff}) with photon energy (MeV) for all S1–S4 glasses is shown in Figure 11. Due to the predominance of photoelectric interaction in this energy zone, the greatest Z_{eff} values were observed here. In the lowest energy range, a considerable increase in Z_{eff} was observed due to the increase in Z (Bi = 83) in the glass matrix. Following that, due to the frequency of Compton scattering, the Z_{eff} values in the intermediate zone decreased considerably. Finally, the growth of Z_{eff} was seen in the most energy-intensive site as a consequence of the bulk of the phenomena related to steam production. This ensures that the S4 with the largest mass attenuation coefficients has the maximum Z_{eff} feasible. The effective atomic number

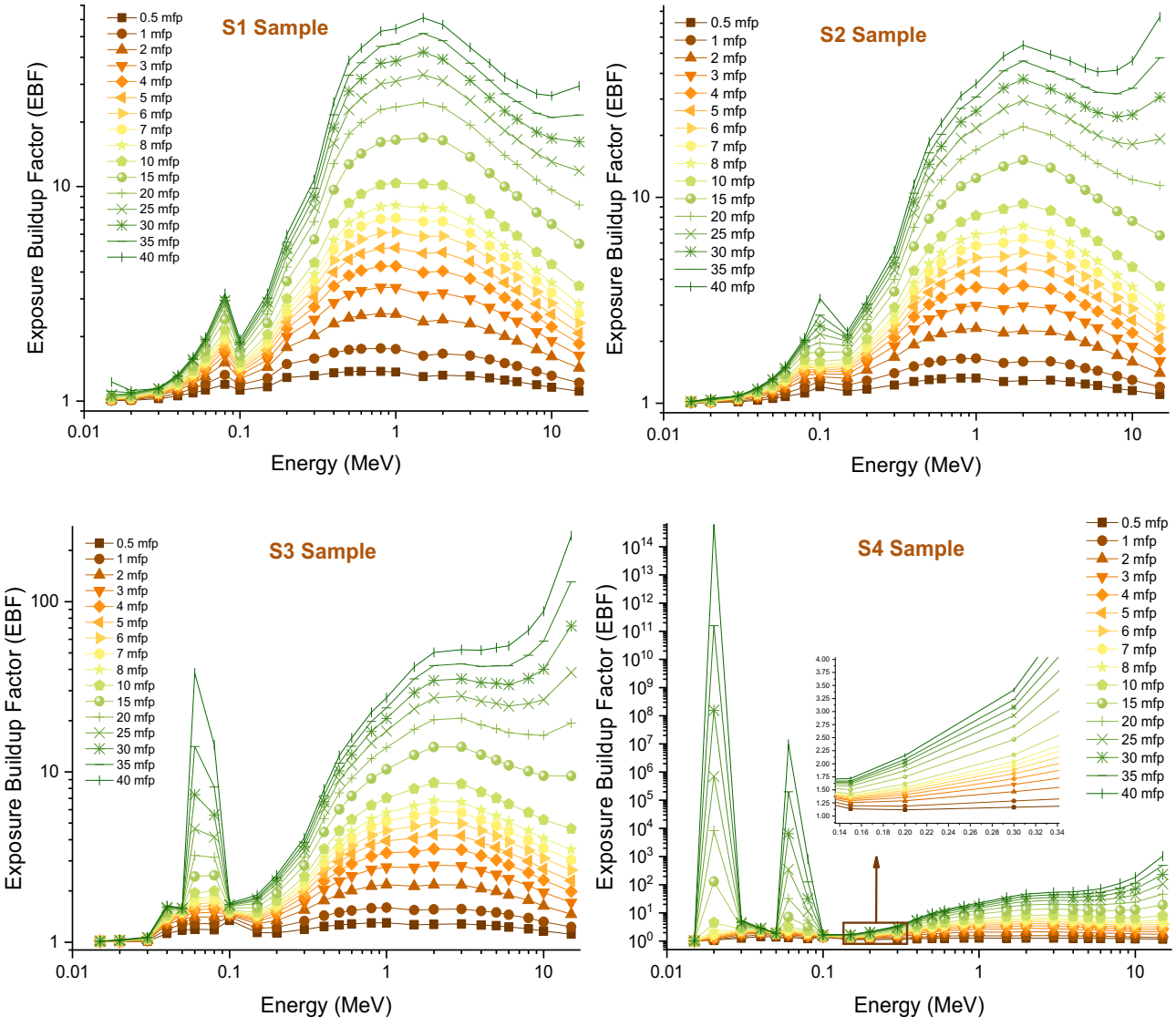

Figure 13: Variation of EBFs of investigated glasses at different mfp values.

(Z_{eff}) is proportional to the effective electron density (N_{eff}), which is stated in terms of electrons per mass unit [40]. The N_{eff} values of the S1, S2, S3, and S4 glasses were determined in this research using the compound concept for the multi-element glass samples. Figure 12 depicts the variation in effective electron density (electrons/g) with photon energy (MeV) for all S1–S4 glasses. The fact that the effective atomic number (Z_{eff}) value and the effective electron density (N_{eff}) values are directly proportional to each other caused the N_{eff} values to show a similar tendency in the energy-dependent change. The results suggested that the S4 sample, which has the highest numerical values for the effective atomic number, has the highest values for effective electron density, theoretically proving the association between these two parameters. The phrase buildup factor (E, x) is frequently used to refer to the percentage of total exposure to un-scattered radiation. Accordingly, the buildup factor may be considered a critical metric to consider when designing radioactive shielding sources such as nuclear reactors. Similarly, for medical radiation protection equipment, the buildup factor is remarkable for gaining a better understanding of the material's total interaction with incoming gamma rays. It is often utilized to determine the amount of gamma irradiation absorbed by equipment underutilization. When absorption is dominating, or the scattering cross-section decreases, the buildup factors exceed or approach unity. There are two types of buildup factors that may be expressed as exposure buildup factor (EBF) and energy absorption buildup factor (EABF). The first one, namely, EBF is defined as the photon accumulation ratio when the exposure is the desired amount and the detector response function is air absorption. On the other hand, the term EABF is sometimes defined as the photon accumulation factor multiplied by the quantity of energy absorbed or deposited in the investigated substance. The variation in

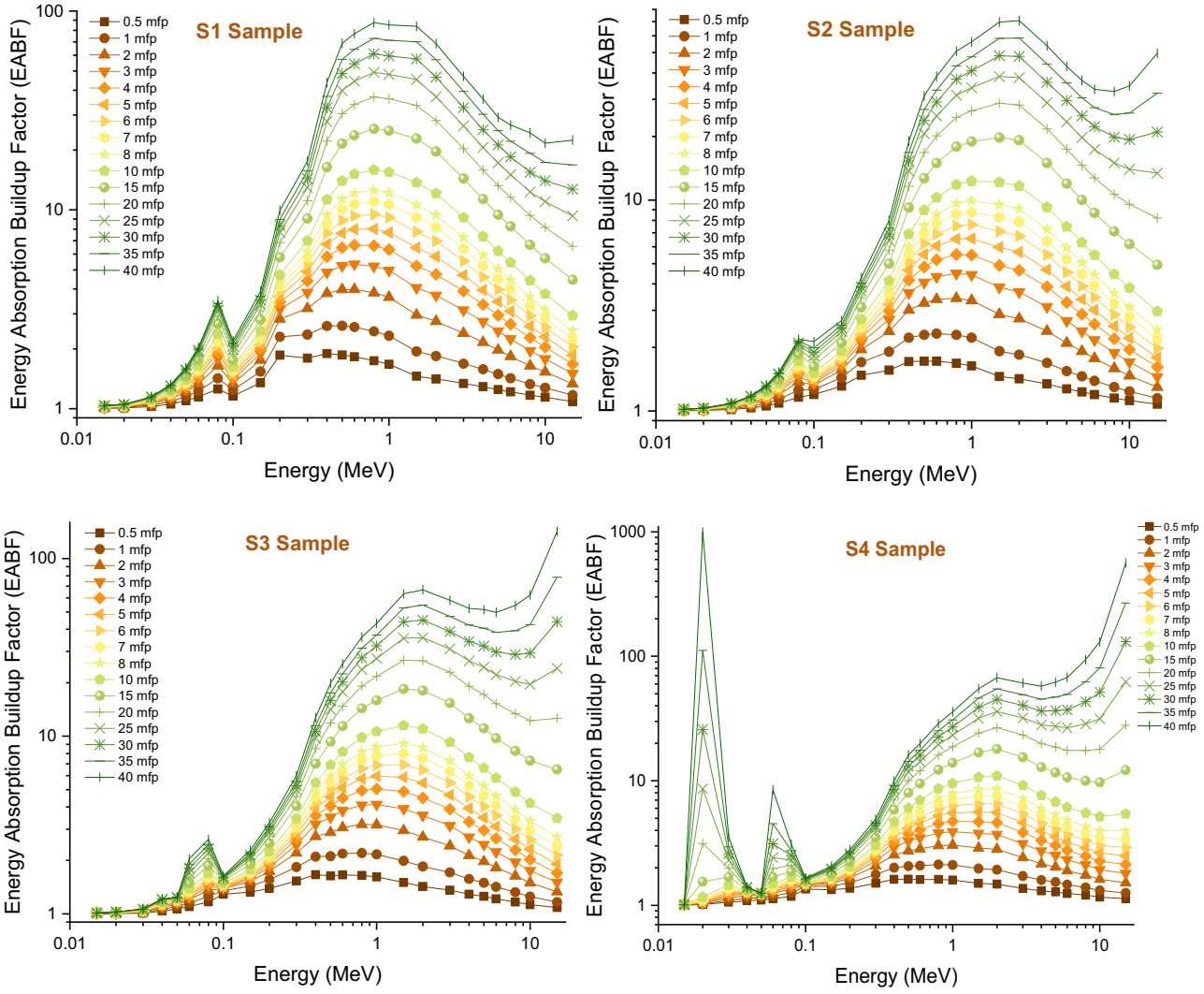

Figure 14: Variation of EABF of investigated glasses at different mean free path values.

EBF and EABF values as a function of gamma-ray energy (MeV) along different mfp values is shown in Figures 13 and 14. As can be seen, both EBF and EABF values are exceedingly low in the low gamma-ray energy area due to the photoelectric interaction's dominance in the absorption of the vast amount of incoming gamma rays. However, at around 0.1 MeV, when Compton scattering becomes dominant, the EBF and EABF values significantly increase. Our findings indicate that increasing the amount of Bi_2O_3 reinforcement decreased the EBF and EABF values for all mfp values (i.e., from 0.5 to 40 mfp). In other words, the collision rate of incoming gamma rays significantly increased in the glass samples as a result of the increase in the amount of Bi from S1 to S4. Finally, another critical parameter for shielding materials, the gamma-ray TF, was determined for S1, S2, S3, S4, and S5 glass samples at various well-known radioisotope energies, such as 0.0086 MeV (Ga-67), 0.0093 MeV (Ga-67), 0.0144 MeV (Co-57), 0.0230 MeV (In-111), 0.0532 MeV (Ba-133), 0.0710 MeV (Tl-201), 0.0796 MeV (Ba-133), 0.0810 MeV (Ba-133), 0.1221 MeV (Co-57), 0.1350 MeV (Tl-201), 0.1365 MeV (Co-57), 0.1405 MeV (Tc-99m), 0.1670 MeV (Tl-201), 0.1710 MeV (In-111), 0.1840 MeV (Ga-67), 0.2450 MeV (In-111), 0.2764 MeV (Ba-133), 0.2843 MeV (I-131), 0.3029 MeV (Ba-133), 0.3201 MeV (Cr-51), 0.3560 MeV (Ba-133), 0.3645 MeV (I-131), 0.3838 MeV (Ba-133), 0.5110 MeV (Co-58), 0.6370 MeV (I-131), 0.6617 MeV (Cs-137), 0.7229 MeV (I-131), 0.8108 MeV (Co-58), 1.1732 MeV (Co-60), and 1.3325 MeV (Co-60). Two processes were used to determine the TF values of the examined glasses. First, we measured the TF factors of S1, S2, S3, and S4 samples at various glass thicknesses. The TFs of studied glasses are shown as a result of the radioisotope energy (MeV) employed at various glass thicknesses, as shown in Figure 15. It is seen that as the radioisotope energy increases from 0.0086 to 1.3326 MeV, the TF

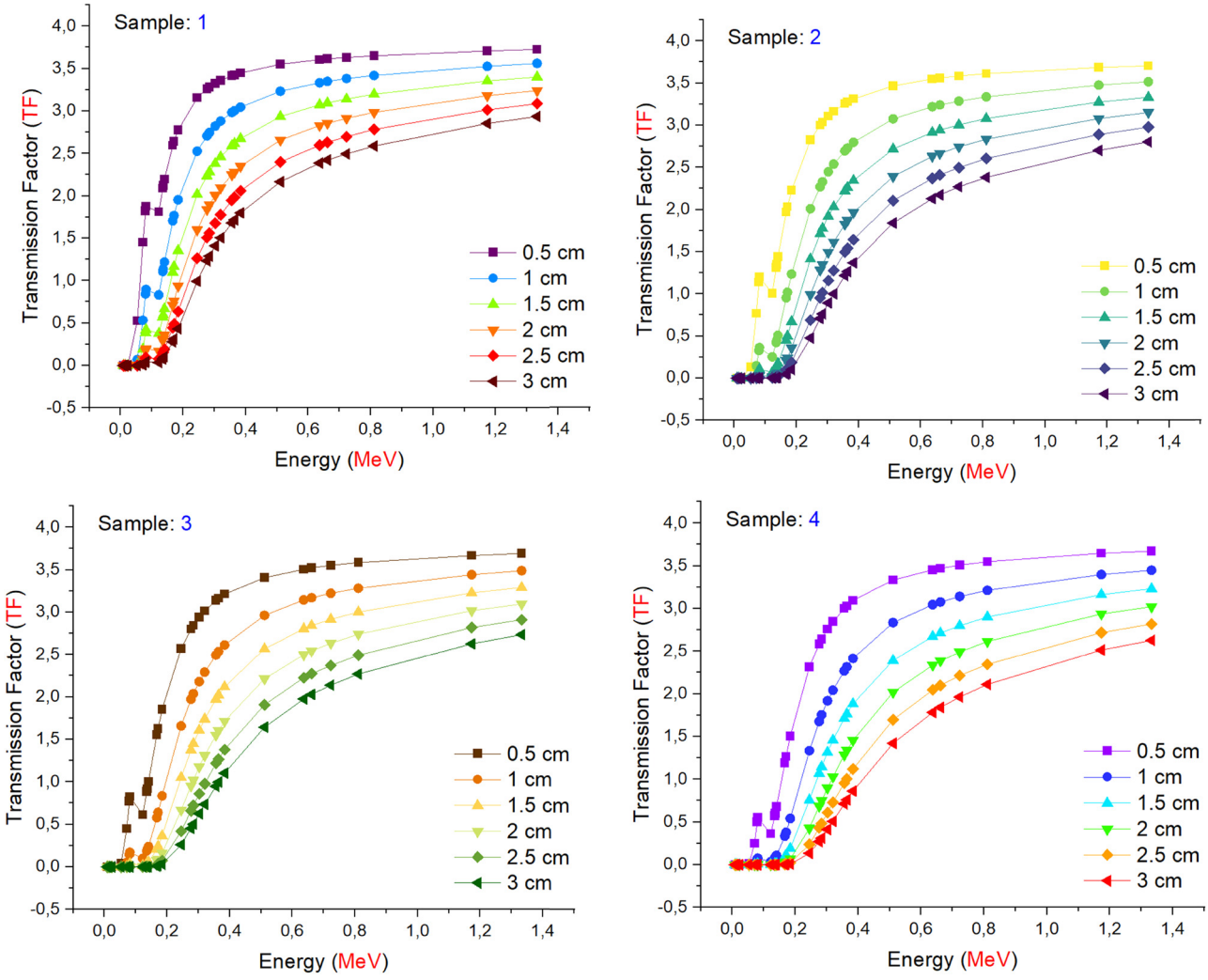

Figure 15: TFs of investigated glasses as a function of used radioisotope energy (MeV) at different glass thicknesses.

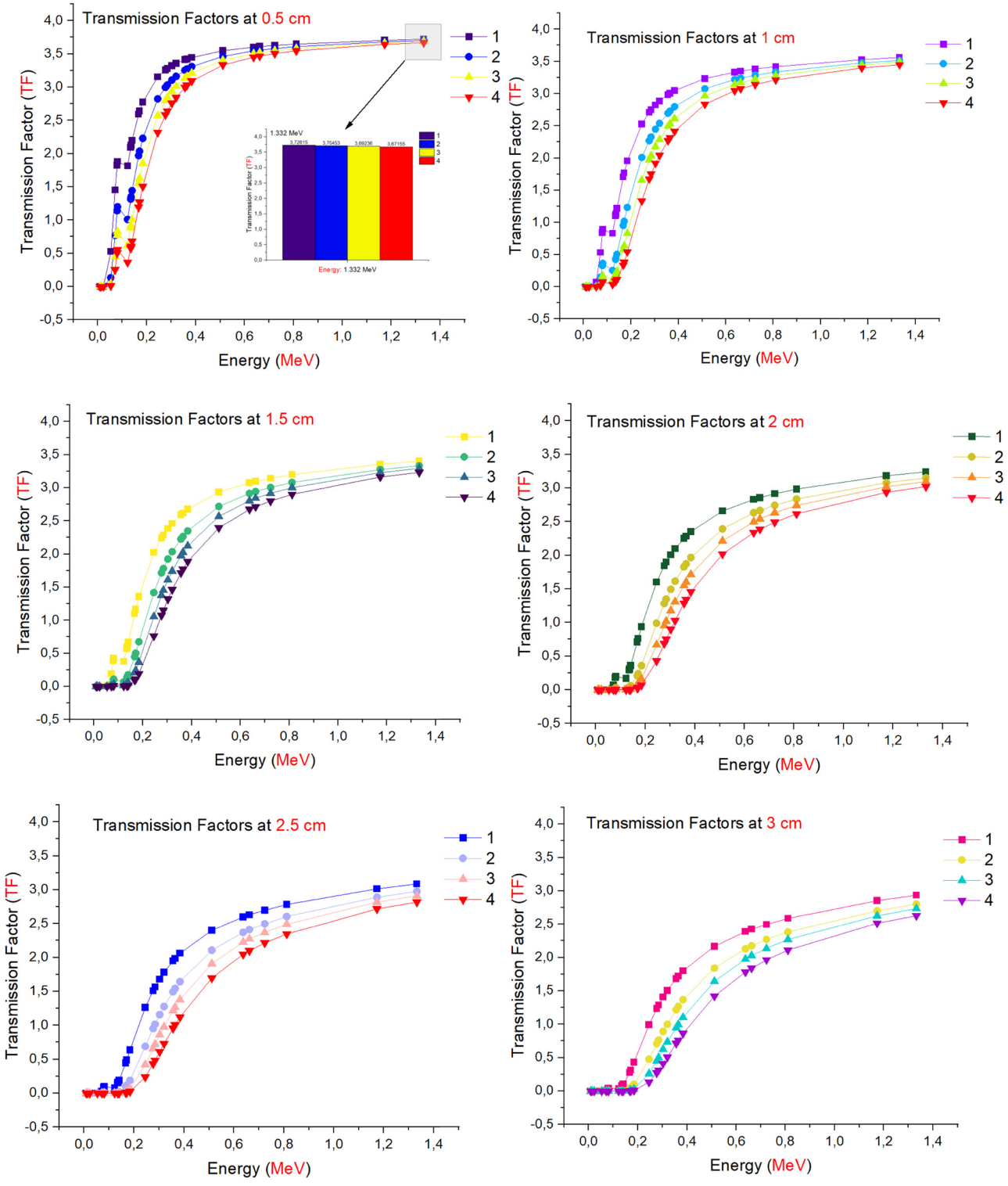

Figure 16: Comparison of the TFs as a function of used radioisotope energy (MeV) for different glass thicknesses.

increases, correspondingly. The glass samples showed the lowest TF values in the low-energy region for all thicknesses. This is because these thick samples have high attenuation capacity for low-energy gamma rays. However, at around 0.1 MeV, a significant separation appears. After 0.1 MeV, glass samples with varying thicknesses begin to behave differentially to incoming gamma rays. Maximum attenuation (also known as minimum transmission) values were

determined for all glass samples studied at a thickness of 3 cm. This condition is explained by the fact that the shield thickness influences the attenuation capacities of any shielding material, implying that increasing shield thickness increases incoming gamma-ray attenuation. Following that the TF values of the studied glasses were assessed extensively by comparing their attenuation capacities throughout various glass thicknesses, including 0.5, 1, 1.5, 2, 2.5, and 3 cm. Figure 16 compares the TFs of various glass thicknesses as a function of the radioisotope energy (MeV) employed. As can be observed, the TF values vary as the incoming gamma-ray energy increases at all thicknesses. Additionally, the minimum TF values for all glass samples were recorded at a thickness of 3 cm. However, the S4 sample exhibited the least transmission behaviors across all glass thicknesses examined.

4 Conclusion

Multidisciplinary approaches to technology and materials sciences that have been developed globally have also allowed the use of many kinds of novel materials in areas other than their conventional applications. One of the best examples of this situation is the use of high-featured and strengthened glass materials as a shielding material in medical, industrial, and research radiation fields. According to the purpose of use and the type of radiation field to be used, it is necessary to characterize each glass material in detail and determine its properties before use. In the current study, the gamma-ray- and neutron-beam-shielding properties of Bi_2O_3–P_2O_5–B_2O_3–V_2O_5 quaternary glass systems with chemical composition $(0.25–x)Bi_2O_3–xB_2O_3–0.75(50\%\ P_2O_5–50\%\ V_2O_5)$, where x = 0.05 (S1), 0.10 (S2), 0.15 (S3), and 0.20 (S4) mol%, and the physical and mechanical aspects of the investigated glasses have been determined and described. Results reveal the following:

1. Values of the packing density (V_t) decreased from 0.634432 for the S1 glass sample to 0.600611 for the S4 glass sample. Values of the dissociation energy (G_t) increased from 51.6125 kJ/cm^3 for the S1 glass sample (with Bi_2O_3 = 5 mol%) to 56.7525 kJ/cm^3 for the S4 glass sample (with Bi_2O_3 = 20 mol%).
2. The mechanical properties were enhanced by increasing the Bi_2O_3 content in the glasses.
3. Linear (μ) and mass attenuation (μ_m) coefficients for the S4 glass sample were the greatest among the glass materials investigated, i.e., $(\mu, \mu_m)_{S1} < (\mu, \mu_m)_{S2} < (\mu, \mu_m)_{S3} < (\mu, \mu_m)_{S4}$.
4. HVL and TVL value for the S4 glass sample were the lowest among all investigated glasses. Therefore, $(HVL, TVL)_{S1} > (HVL, TVL)_{S2} > (HVL, TVL)_{S3} > (HVL, TVL)_{S4}$.
5. The effective atomic number (Z_{eff}) of the investigated glasses showed the same trend for linear and mass attenuation coefficients.
6. The effective electron density (N_{eff}) values of glasses had a similar tendency to (Z_{eff}) in the energy-dependent manner.
7. Our findings indicated that increasing the amount of Bi_2O_3 reinforcement decreased the EBF and EABF values for all mfp values (i.e., from 0.5 to 40 mfp).
8. The minimum TF values for all glass samples were recorded at a thickness of 3 cm. However, the S4 sample exhibited the least transmission behaviors across all glass thicknesses examined.

According to the study's findings, it can be concluded that such glass materials, some of whose critical material characteristics were evaluated, may be employed as shielding materials in accordance with existing standards and physical limitations associated with the energy ranges utilized. On the other hand, it may be beneficial to investigate how the optical qualities and potential drawbacks of these materials may be enhanced for diagnostic radiology rooms, reactor areas, and other applications requiring high optical transmittance. Finally, it can be concluded that certain kinds of radiation, such as alpha, proton, and neutron, are worth further investigating. On the other hand, mechanical and thermal properties and elastic moduli are also worth further investigating because durability and thermal conductivity are other important properties for any shielding material.

Funding information: This work was performed under Princess Nourah bint Abdulrahman University Researchers' Supporting Project (No. PNURSP2022R149), Princess Nourah bint Abdulrahman University, Riyadh, Saudi Arabia. The authors express their sincere gratitude to Princess Nourah bint Abdulrahman University.

Author contributions: H.O.T., A.B., H.M.H.Z., and S.A.M.I.; methodology: G.K., H.O.T.; software: H.O.T., G.L., H.M.H.Z., and A.E.; validation: S.A.M.I., Y.S.R., and A.E.; formal analysis: G.K., Y.S.R., H.M.H.Z., and G.S.; investigation: G.K. and H.O.T.; resources: G.K., G.S., and A.B.; data curation: S.A.M.I. and A.E.; writing – original draft preparation: H.O.T., G.S., G.L., Y.S.R., and A.W.; writing – review and editing: H.M.H.Z., S.A.M.I., and A.E.; visualization: Y.S.R. and G.S.; supervision: H.M.H.Z. and A.B.; project administration: H.O.T. and S.A.M.; funding acquisition:

A.E. (The authors thank the "Dunarea de Jos" University of Galati, Romania, for the APC support.) All authors have read and agreed to the published version of the manuscript.

Conflict of interest: The authors declare no conflict of interest.

Ethical approval: The conducted research is not related to either human or animal use.

Data availability statement: The data presented in this study are available on request from the corresponding author.

References

[1] Kim JH. Three principles for radiation safety: time, distance, and shielding. Korean J Pain. 2018;31:145. doi: 10.3344/KJP.2018.31.3.145.

[2] Tishkevich DI, Grabchikov SS, Grabchikova EA, Vasin DS, Lastovskiy SB, Yakushevich AS, et al. Modeling of paths and energy losses of high-energy ions in single-layered and multilayered materials. IOP Conf Ser Mater Sci Eng. 2020;848:012089. doi: 10.1088/1757-899X/848/1/012089.

[3] Sayyed MI, Albarzan B, Almuqrin AH, El-Khatib AM, Kumar A, Tishkevich DI, et al. Experimental and theoretical study of radiation shielding features of $CaO–K_2O–Na2_O–P_2O_5$ glass systems. Mater. 2021;14:3772. doi: 10.3390/MA14143772.

[4] Sayyed MI, Askin A, Zaid MHM, Olukotun SF, Khandaker MU, Tishkevich DI, et al. Radiation shielding and mechanical properties of $Bi_2O_3–Na_2O–TiO_2–ZnO–TeO_2$ glass system. Radiat Phys Chem. 2021;186:109556. doi: 10.1016/J.RADPHYSCHEM.2021.109556.

[5] Tishkevich DI, Grabchikov SS, Lastovskii SB, Trukhanov SV, Zubar TI, Vasin DS, et al. Effect of the synthesis conditions and microstructure for highly effective electron shields production based on Bi coatings. ACS Appl Energy Mater. 2018;1:1695–702. doi: 10.1021/ACSAEM.8B00179.

[6] Kavaz E, Yorgun NY. Gamma ray buildup factors of lithium borate glasses doped with minerals. J Alloy Compd. 2018;752:61–7. doi: 10.1016/j.jallcom.2018.04.106.

[7] Tekin HO, ALMisned G, Susoy G, Zakaly HMH, Issa SAM, Kilic G, et al. A detailed investigation on highly dense CuZr bulk metallic glasses for shielding purposes. Open Chem. 022;20:69–80. doi: 10.1515/chem-2022-0127.

[8] Tekin HO, ALMisned G, Zakaly HMH, Zamil A, Khoucheich D, Bilal G, et al. Gamma, neutron, and heavy charged ion shielding properties of Er^{3+}-doped and Sm^{3+}-doped zinc borate glasses. Open Chem. 2022;20:130–45. doi: 10.1515/CHEM-2022-0128.

[9] Ramteke DD, Annapurna K, Deshpande VK, Gedam RS. Effect of Nd^{3+} on spectroscopic properties of lithium borate glasses. J Rare Earths. 2014;32:1148–53. doi: 10.1016/S1002-0721(14)60196-4.

[10] Rashad M, Saudi HA, Zakaly HMH, Issa SAM, Abd-Elnaiem AM. Control optical characterizations of Ta + 5–doped B2O3–Si2O–CaO–BaO glasses by irradiation dose. Opt Mater (Amst). 2021;112:110613. doi: 10.1016/j.optmat.2020.110613.

[11] Tekin HO, Susoy G, Issa SAM, Ene A, ALMisned G, Rammah YS, et al. Heavy Metal Oxide (HMO) glasses as an effective member of glass shield family: A comprehensive characterization on gamma ray shielding properties of various structures. J Mater Res Technol. 2022;18:231–44. doi: 10.1016/J.JMRT.2022.02.074.

[12] Lakshminarayana G, Elmahroug Y, Kumar A, Tekin HO, Rekik N, Dong M, et al. Detailed inspection of γ-ray, fast and thermal neutrons shielding competence of calcium oxide or strontium oxide comprising bismuth borate glasses. Mater (Basel). 2021;14:2265. doi: 10.3390/ma14092265.

[13] Alsaif NAM, Rekik N, Elmahroug Y, Lakshminarayana G, Farooq U, Affan H, et al. Simulating the γ-ray and neutron attenuation properties of lithium borate glasses doped barite: efficient and deterministic analysis using relevant simulation codes. J Mater Res Technol. 2022;17:679–99. doi: 10.1016/j.jmrt.2022.01.021.

[14] Alsaif NAM, Elmahroug Y, Alotaibi BM, Alyousef HA, Rekik N, Hussein AWMA, et al. Calculating photon buildup factors in determining the γ-ray shielding effectiveness of some materials susceptible to be used for the conception of neutrons and γ-ray shielding. J Mater Res Technol. 2021;11:769–84. doi: 10.1016/j.jmrt.2021.01.052.

[15] Kassab LRP, da Silva Mattos GR, Issa SAM, Bilal G, Bordon CDS, Kilic G, et al. Optical and physical behaviours of newly developed germanium-tellurium (GeTe) glasses: a comprehensive experimental and in-silico study with commercial glasses and ordinary shields. J Mater Sci Mater Electron. 2021;32:22953–73. doi: 10.1007/S10854-021-06780-Y.

[16] Issa SAM, Zakaly HMH, Badawi A, Elsaman R, Tekin HO, Showahy AA, et al. An experimental investigation on structural, mechanical and physical properties of Strontium–Silicon Borate glass system through Bismuth-Aluminum substitution. Opt Mater (Amst). 2021;117:111124. doi: 10.1016/j.optmat.2021.111124.

[17] Zhukovsky M, Koubisy MSI, Zakaly HMH, Ali AS, Issa SAM, Tekin HO. Dielectric, structural, optical and radiation shielding properties of newly synthesized $CaO–SiO_2–Na_2O–Al_2O_3$ glasses: experimental and theoretical investigations on impact of Tungsten(III) oxide. Appl Phys A. 2022;128:205. doi: 10.1007/S00339-022-05328-Z.

[18] Sung W, Won J, Lee J, Kim H. Properties and structure of $P_2O_5–V_2O_5–ZnO/B_2O_3$ glasses. Mol Cryst Liq Cryst. 2009;499:234/[556]–241/[563]. doi: 10.1080/15421400802619891.

[19] Abd-Elnaiem AM, Saudi HA, Zakaly HMH, Issa SAM, Rashad M. The effect of composition and γ-irradiation on the Vickers hardness, structural and optical properties of xLiNbO$_3$–25CaO–$_{35}$PbO-(40-x) waste systems. Ceram Int. 2021;47:18751–60. doi: 10.1016/j.ceramint.2021.03.210.

[20] He D, Fang Y, Liao M, Zhao G, Sun Y, Yu F, et al. Luminescence properties and energy transfer behavior of Dy3+/Tm3+ co-doped phosphate glasses with high moisture-resistance and thermal stability for W-LEDs. J Lumin. 2021;236:118087. doi: 10.1016/j.jlumin.2021.118087.

[21] Koudelka L, Mošner P. Study of the structure and properties of Pb-Zn borophosphate glasses. J Non Cryst Solids. 2001;293–295:635–41. North-Holland. doi: 10.1016/S0022-3093(01)00765-7.

[22] Lim JW, Schmitt ML, Brow RK, Yung SW. Properties and structures of tin borophosphate glasses. J Non Cryst Solids. 2010;356:1379–84. doi: 10.1016/j.jnoncrysol.2010.02.019.

[23] Szumera M, Wacławska I, Olejniczak Z. Influence of B2O3 on the structure and crystallization of soil active glasses. J Therm Anal Calorim. 2010;99:879–86. doi: 10.1007/s10973-009-0550-1.

[24] Baikova LG, Fedorov YK, Pukh VP, Tikhonova LV, Kazannikova TP, Sinani AB, et al. Influence of Boron Oxide on the Physicomechanical Properties of Glasses in the Li_2O–B_2O_3–P_2O_5 system. Glas Phys Chem. 2003;29:276–81. doi: 10.1023/A:1024486116145.

[25] Liu SJ, Lu AX, Tang XD, He SB. Influence of addition of B_2O_3 on properties of Yb3+ -doped phosphate laser glass. J Cent South Univ Technol (Engl Ed). 2006;13:468–72. doi: 10.1007/s11771-006-0069-6.

[26] Muñoz F, Montagne L, Pascual L, Durán A. Composition and structure dependence of the properties of lithium borophosphate glasses showing boron anomaly. J Non Cryst Solids. 2009;355:2571–7. doi: 10.1016/j.jnoncrysol.2009.09.013.

[27] Mošner P, Koudelka L. Glass-Forming ability, thermal stability and chemical durability of lead borophosphate glasses. Phosphorus Res Bull. 2002;13:197–200. doi: 10.3363/prb1992.13.0_197.

[28] Donald IW, Metcalfe BL, Bradley DJ, Hill MJC, McGrath JL, Bye AD. The preparation and properties of some lithium borate based glasses. J Mater Sci. 1994;29:6379–96. doi: 10.1007/BF00353994.

[29] Saranti A, Koutselas I, Karakassides MA. Bioactive glasses in the system CaO–B_2O_3–P_2O_5: Preparation, structural study and in vitro evaluation. J Non Cryst Solids. 2006;352:390–8. doi: 10.1016/j.jnoncrysol.2006.01.042.

[30] Rammah YS, Olarinoye IO, El-Agawany FI, Yousef ES, Ibrahim S, Ali AA. SrO-reinforced potassium sodium borophosphate bioactive glasses: Compositional, physical, spectral, structural properties and photon attenuation competence. J Non Cryst Solids. 2021;559:120667. doi: 10.1016/J.JNONCRYSOL.2021.120667.

[31] Ravikumar RVSSN, Rajagopal Reddy V, Chandrasekhar AV, Reddy BJ, Reddy YP, Rao PS. Tetragonal site of transition metal ions doped sodium phosphate glasses. J Alloy Compd. 2002;337:272–6. doi: 10.1016/S0925-8388(01)01963-6.

[32] Srinivas B, Hameed A, Shareefuddin M, Chary MN. EPR and optical studies of BaO–TeO_2–TiO_2–B_2O_3 glasses containing V4+ and Cu2+ transitional metal ion. Mater. Today Proc. 2015;2:1915–22. Elsevier Ltd. doi: 10.1016/j.matpr.2015.07.151.

[33] Kerkouri N, Et-Tabirou M, Chahine A, Mazzah A, Dhamelincourt MC, Taibi M. DSC and spectroscopic studies of the structure of V_2O_5–CdO–P_2O_5 glasses. J Optoelectron Adv Mater. 2010;12:1030–4.

[34] Rammah YS, Issa SAM, Zakaly HMH, Tekin HO, Yousef E, Abouhaswa AS. B_2O_3–Bi_2O_3–Li_2O_3–Cr_2O_3 glasses: fabrication, structure, mechanical, and gamma radiation shielding qualities. J Aust Ceram Soc. 2021;57:1057–69. doi: 10.1007/s41779-021-00599-w.

[35] Işsever UG, Kilic G, Peker M, Ünaldi T, Aybek AŞ. Effect of low ratio V5+ doping on structural and optical properties of borotellurite semiconducting oxide glasses. J Mater Sci Mater Electron. 2019;30:15156–67. doi: 10.1007/S10854-019-01889-7/TABLES/5.

[36] Şakar E, Özpolat ÖF, Alım B, Sayyed MI, Kurudirek M. Phy-X/PSD: Development of a user friendly online software for calculation of parameters relevant to radiation shielding and dosimetry. Radiat Phys Chem. 2020;166:108496. doi: 10.1016/j.radphyschem.2019.108496.

[37] Rammah YS, Tekin HO, Sriwunkum C, Olarinoye I, Alalawi A, Al-Buriahi MS, et al. Investigations on borate glasses within SBC-Bx system for gamma-ray shielding applications. Nucl Eng Technol. 2021;53:282–93. doi: 10.1016/J.NET.2020.06.034.

[38] Abouhaswa AS, El-Agawany FI, Ahmed EM, Rammah YS. Optical, magnetic characteristics, and nuclear radiation shielding capacity of newly synthesized barium boro-vanadate glasses: B_2O_3–BaF_2–Na_2O–V_2O_5. Radiat Phys Chem. 2022;192:109922. doi: 10.1016/j.radphyschem.2021.109922.

[39] Zakaly HM, Ashry A, El-Taher A, Abbady AGE, Allam EA, El-Sharkawy RM, et al. Role of novel ternary nanocomposites polypropylene in nuclear radiation attenuation properties: In-depth simulation study. Radiat Phys Chem. 2021;188:109667. doi: 10.1016/j.radphyschem.2021.109667.

[40] Barebita H, Ferraa S, Moutataouia M, Baach B, Elbadaoui A, Nimour A, et al. Structural investigation of Bi_2O_3–P_2O_5–B_2O_3–V_2O_5 quaternary glass system by Raman, FTIR and thermal analysis. Chem Phys Lett. 2020;760:138031. doi: 10.1016/j.cplett.2020.138031.

[41] Makishima A, Mackenzie JD. Direct calculation of Young's modulus of glass. J Non Cryst Solids. 1973;12:35–45. doi: 10.1016/0022-3093(73)90053-7.

[42] Saddeek YB, Zakaly HM, Sekhar KC, Issa SA, Alharbi T, Badawi A, et al. Investigations of mechanical and radiation shielding properties of $BaTiO_3$-modified cadmium alkali borate glass. Appl Phys A. 2022;128:1–10. doi: 10.1007/S00339-022-05413-3.

[43] Inaba S, Fujino S, Morinaga K. Young's modulus and compositional parameters of oxide glasses. J Am Ceram Soc. 1999;82:3501–7. doi: 10.1111/j.1151-2916.1999.tb02272.x.

[44] Rammah YS, Olarinoye IO, El-Agawany FI, El-Adawy A, Gamal A, Yousef ES. Elastic moduli, photon, neutron, and proton shielding parameters of tellurite bismo-vanadate (TeO_2–V_2O_5–Bi_2O_3) semiconductor glasses. Ceram Int. 2020;46:25440–52. doi: 10.1016/j.ceramint.2020.07.014.

[45] Elkhoshkhany N, Syala E, Sayed Yousef E. Concentration dependence of the elastic moduli, thermal properties, and non-isothermal kinetic parameters of Yb3+ doped multicomponent tellurite glass system. Results Phys. 2020;16:102876. doi: 10.1016/j.rinp.2019.102876.

[46] Tekin HO, ALMisned G, Susoy G, Ali FT, Baykal DS, Ene A, et al. Transmission factor (TF) behavior of Bi_2O_3–TeO_2–Na_2O–TiO_2–ZnO glass system: A Monte Carlo simulation study. Sustainability. 2022;14:2893. doi: 10.3390/su14052893.

[47] RSICC Computer Code Collection, MCNPX User's Manual Version 2.4.0. MonteCarlo N-particle transport code system for multiple and high energy applications; 2002. Google Search n.d. https://www.google.com/search?q=RSICC+Computer+Code+Collection%2C+MCNPX+User%27s+Manual+Version

+2.4.0.+MonteCarlo+N-Particle+Transport+Code+System+for+Multiple+and+High+Energy+Applications%2C(2002).&oq=RSICC+Computer+Code+Collection%2C+MCNPX+User%27s+Manu (accessed December 31, 2020).

[48] Saudi HA, Zakaly HMH, Issa SAM, Tekin HO, Hessien MM, Rammah YS, et al. Fabrication, FTIR, physical characteristics and photon shielding efficacy of CeO_2/sand reinforced borate glasses: Experimental and simulation studies. Radiat Phys Chem. 2022;191:109837. doi: 10.1016/j.radphyschem.2021.109837.

[49] Kaginelli S, Rajeshwari T, Sharanabasappa, Kerur B, Kumar A. Effective atomic numbers and electron density of dosimetric material. J Med Phys. 2009;34:176–9. Wolters Kluwer: Medknow Publications. doi: 10.4103/0971-6203.54853.

[50] Akkurt I, Boodaghi Malidarre R. Gamma photon-neutron attenuation parameters of marble concrete by MCNPX code. Radiat Eff Defects Solids. 2021;176:906–18. doi: 10.1080/10420150.2021.1975708.

[51] Akkurt I, Tekin HO. Radiological parameters of bismuth oxide glasses using the Phy-X/PSD software. Emerg Mater Res. 2020;9:1020–7. doi: 10.1680/jemmr.20.00209.

[52] Rammah YS, Kumar A, Mahmoud KAA, El-Mallawany R, El-Agawany FI, Susoy G, et al. SnO-reinforced silicate glasses and utilization in gamma-radiation-shielding applications. Emerg Mater Res. 2020;9:1000–8. doi: 10.1680/jemmr.20.00150.

[53] Tekin HO, Issa SAM, Mahmoud KAA, El-Agawany FI, Rammah YS, Susoy G, et al. Nuclear radiation shielding competences of barium-reinforced borosilicate glasses. Emerg Mater Res. 2020;9:1131–44. doi: 10.1680/jemmr.20.00185.

[54] Çelen YY. Gamma-ray-shielding parameters of some phantom fabrication materials for medical dosimetry. Emerg Mater Res. 2021;10:307–13. doi: 10.1680/jemmr.21.00043.

[55] Zakaly HMH, Rashad M, Tekin HO, Saudi HA, Issa SAM, Henaish AMA. Synthesis, optical, structural and physical properties of newly developed dolomite reinforced borate glasses for nuclear radiation shielding utilizations: An experimental and simulation study. Opt Mater (Amst). 2021;114110942. doi: 10.1016/j.optmat.2021.110942.

[56] Çelen YY, Evcin A. Synthesis and characterizations of magnetite-borogypsum for radiation shielding. Emerg Mater Res. 2020;9:770–5. doi: 10.1680/jemmr.20.00098.

[57] ALMisned G, Elshami W, Issa SAM, Susoy G, Zakaly HMH, Algethami M, et al. Enhancement of Gamma-ray shielding properties in Cobalt-Doped heavy metal borate glasses: The role of lanthanum oxide reinforcement. Mater. 2021;14:7703. doi: 10.3390/MA14247703.